Composition controlled spin polarization in $Co_{1-x}Fe_xS_2$ alloys

2007 J. Phys.: Condens. Matter 19 315219

(http://iopscience.iop.org/0953-8984/19/31/315219)

IOP PUBLISHING JOURNAL OF PHYSICS: CONDENSED MATTER

J. Phys.: Condens. Matter **19** (2007) 315219 (22pp) doi:10.1088/0953-8984/19/31/315219

Composition controlled spin polarization in $Co_{1-x}Fe_xS_2$ alloys

C Leighton[1,9], M Manno[1], A Cady[2], J W Freeland[2], L Wang[1,3], K Umemoto[1,4], R M Wentzcovitch[1,4], T Y Chen[5], C L Chien[5], P L Kuhns[6], M J R Hoch[6], A P Reyes[6], W G Moulton[6], E D Dahlberg[7], J Checkelsky[8] and J Eckert[8]

[1] Department of Chemical Engineering and Materials Science, University of Minnesota, USA
[2] Advanced Photon Source, Argonne National Laboratory, USA
[3] School of Physical and Mathematical Science, Nanyang Technological University, Singapore
[4] Supercomputer Institute, University of Minnesota, USA
[5] Department of Physics and Astronomy, Johns Hopkins University, USA
[6] National High Magnetic Field Laboratory, Florida State University, USA
[7] School of Physics and Astronomy, University of Minnesota, USA
[8] Physics Department, Harvey Mudd College, USA

E-mail: Leighton@umn.edu

Received 16 November 2006
Published 3 July 2007
Online at stacks.iop.org/JPhysCM/19/315219

Abstract

The transition metal (TM) chalcogenides of the form TMX_2 (X = S or Se) have been studied for decades due to their interesting electronic and magnetic properties such as metamagnetism and metal–insulator transitions. In particular, the $Co_{1-x}Fe_xS_2$ alloys were the subject of investigation in the 1970s due to general interest in itinerant ferromagnetism. In recent years (2000–present) it has been shown, both by electronic structure calculations and detailed experimental investigations, that $Co_{1-x}Fe_xS_2$ is a model system for the investigation of highly spin polarized ferromagnetism. The radically different electronic properties of the two endpoint compounds (CoS_2 is a narrow bandwidth ferromagnetic metal, while FeS_2 is a diamagnetic semiconductor), in a system forming a substitutional solid solution allows for composition control of the Fermi level relative to the spin split bands, and therefore composition-controlled conduction electron spin polarization. In essence, the recent work has shown that the concept of 'band engineering' can be applied to half-metallic ferromagnets and that high spin polarization can be deliberately engineered. Experiments reveal tunability in both sign and magnitude of the spin polarization at the Fermi level, with maximum values obtained to date of 85% at low temperatures. In this paper we review the properties of $Co_{1-x}Fe_xS_2$ alloys, with an emphasis on properties of relevance to half-metallicity. Crystal structure, electronic structure, synthesis, magnetic

[9] Author to whom any correspondence should be addressed.

properties, transport properties, direct probes of the spin polarization, and measurements of the total density of states at the Fermi level are all discussed. We conclude with a discussion of the factors that influence, or even limit, the spin polarization, along with a discussion of opportunities and problems for future investigation, particularly with regard to fundamental studies of spintronic devices.

(Some figures in this article are in colour only in the electronic version)

1. Introduction

The emerging research field of spin-electronics, or *spintronics*, has received a great deal of attention in recent years [1, 2]. As opposed to conventional microelectronics, where only the electronic charge is manipulated, both charge *and* spin are utilized in spintronics. 'First-generation' spintronic devices are already in existence and are currently used, or are under development, in the magnetic recording industry. Examples include spin-valve and current perpendicular to the plane giant magnetoresistance (GMR) read heads [1–4] and non-volatile magnetic random access memory (MRAM) [1, 2, 5], based on tunnelling magnetoresistance (TMR) [1, 2, 6]. Future generations of spintronic devices promise to combine technologically important non-magnetic semiconductors with magnetism, either by synthesizing dilute magnetic semiconductors or by fabricating heterostructures with conventional ferromagnetic metals [1, 2].

A key component common to all spintronic devices is a source of spin-polarized carriers, most commonly a ferromagnetic (FM) material. It is clear that in many cases the performance of the spintronic devices is dramatically improved if this electron source is highly polarized, i.e. if the polarization of the electron spins at the Fermi level, P, is large. In terms of the electronic band structure, spin polarization is usually defined by [7],

$$P = \frac{N_\uparrow(E_\mathrm{F}) - N_\downarrow(E_\mathrm{F})}{N_\uparrow(E_\mathrm{F}) + N_\downarrow(E_\mathrm{F})}, \tag{1}$$

where $N_{\uparrow,\downarrow}(E_\mathrm{F})$ is the spin-dependent density of states (DOS) at the Fermi level, E_F. Spin polarized photoemission is a technique that is capable of providing such a direct measurement of P, but it suffers from poor energy resolution and surface sensitivity [8–10]. Alternatively, P can be probed by electron tunnelling across an insulating barrier, either using two FM electrodes [6] or one FM and one superconducting electrode (i.e. the Meservey–Tedrow method) [11]. The tunnelling spin polarization is defined as,

$$P = \frac{N_\uparrow(E_\mathrm{F})|T_\uparrow|^2 - N_\downarrow(E_\mathrm{F})|T_\downarrow|^2}{N_\uparrow(E_\mathrm{F})|T_\uparrow|^2 + N_\downarrow(E_\mathrm{F})|T_\downarrow|^2}, \tag{2}$$

where $T_{\uparrow,\downarrow}$ is the (potentially spin-dependent) tunnelling matrix element. Planar or point contact Andréev reflection (PCAR) can also be used to measure P [12–20], the relevant definition being,

$$P = \frac{N_\uparrow(E_\mathrm{F})v_{\mathrm{F},\uparrow} - N_\downarrow(E_\mathrm{F})v_{\mathrm{F},\downarrow}}{N_\uparrow(E_\mathrm{F})v_{\mathrm{F},\uparrow} + N_\downarrow(E_\mathrm{F})v_{\mathrm{F},\downarrow}}, \tag{3}$$

where $v_{\mathrm{F}\uparrow,\downarrow}$ is the (potentially spin-dependent) Fermi velocity. If the electronic transport is diffusive, then v_F is replaced with v_F^2. It is therefore important to note that different definitions of P are accessed in different experimental situations [7].

Ferromagnets with $P = 100\%$, also known as half-metallic ferromagnets (HMFs) [21], would be ideal materials for use as a source of polarized spins. Such materials have E_F

located in the conduction band for one spin orientation and in a gap for the opposite spin orientation, resulting in $P = 100\%$. The advantages offered by these HMFs can be seen for example from the theoretical predictions [22], and experimental observations [23–25], of very large TMR in magnetic tunnel junctions as $P \rightarrow 100\%$, as well as the theoretical claims that efficient 'Ohmic' spin injection [26, 27] will only be possible in the limit $P \rightarrow 100\%$ [28]. This situation has led to an intensive search for HMFs. Indeed, several ferromagnets (or ferrimagnets) have been the subject of experimental investigations, concluding that the materials are either highly polarized or truly HMF (at least at low T). CrO_2 [9, 15, 16, 29], Fe_3O_4 [10, 30], $La_{0.67}Sr_{0.33}MnO_3$ [8, 14, 17, 18] and $Ga_{0.95}Mn_{0.05}As$ [31] are perhaps the most widely known examples, where P values lie in the range 80–100% by various techniques. Of these, the strongest evidence, particularly from transport investigations [15, 29], occurs for CrO_2. It should be noted, however, that there still remain some controversies regarding the labelling of any of these compounds as 'half-metallic' [32], particularly at finite temperatures [33, 34]. The fact that different definitions of P apply to different measurement modes (see above), problems with probing interface versus bulk electronic structure, and the fact that spin polarizations derived from photoemission are sensitive to the measurement conditions chosen [32], are just some of the factors contributing to the difficulty in concluding true half-metallicity. There is also a significant amount of theoretical work suggesting that excitations at finite temperatures lead to the destruction of the fully polarized state, even for systems that are half-metallic at $T = 0$ [32–34]. There are several pieces of experimental evidence to support this notion that P is reduced at high temperatures [32, 8].

In addition to these general comments, several of these compounds suffer from key drawbacks such as metastability and incompatibility with conventional vacuum deposition techniques (CrO_2), poor conductivity at low T (Fe_3O_4), low Curie temperature (T_C) ($Ga_{1-x}Mn_xAs$), and rapid fall-off in P with increasing T ($La_{1-x}Sr_xMnO_3$ and CrO_2). Moreover, even in the case of CrO_2, where strong evidence exists for full polarization at low T, the expected large enhancements in TMR have not been obtained. It is therefore clear that it is very important for future progress that other highly polarized materials are developed. In addition, although it has not been discussed in the literature, FM systems with *tunable* P could be very useful for basic research in spintronics [35]. For instance, this would allow for the measurement of the device performance (e.g. TMR) as a controlled function of the spin polarization of the FM electrodes. This is a desirable property, even if the T_C of the material in question is too low for technological applications; it would still allow for fundamental studies of spintronic devices as a function of the spin polarization. In this paper we review the successful application of a simple scheme that allows for composition control over the spin polarization of the ferromagnet $Co_{1-x}Fe_xS_2$ [35].

The basic concept behind the composition control of the E_F position relative to the spin split bands is discussed in the next section (section 2). This is followed by sections dealing with electronic structure, crystal structure and synthesis, basic magnetic properties, electronic transport properties, direct probes of P, and measurement of the total DOS at the E_F. The strong evidence of high, composition-controlled spin polarization from multiple theoretical and experimental probes is emphasized. The paper concludes with a discussion of the factors that influence (or even limit) the polarization, along with a discussion of important directions for future research.

2. The basic concept of Fermi level control in $Co_{1-x}Fe_xS_2$

The band engineering concept is based on the pyrite structure itinerant ferromagnet CoS_2, which has $T_C = 121$ K, electronic configuration $t_{2g}^6 e_g^1$, and $S = 1/2$, i.e. in a simple model a

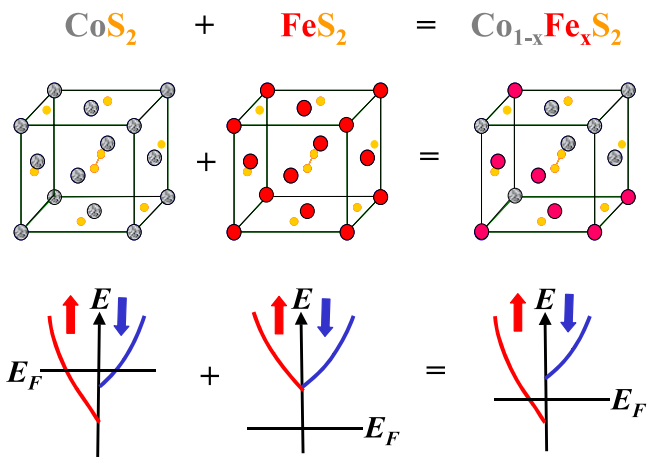

Figure 1. Schematic illustration of the Fermi level control concept. Unit cells and (spin resolved) density of states versus energy diagrams (with the Fermi energies labelled) are shown for CoS_2, FeS_2 and $Co_{1-x}Fe_xS_2$.

single electron would populate the e_g-derived conduction band. The recent finding of $P = 57\%$ from PCAR confirms that this material, in undoped form, is *not* half-metallic [36]. The essential concept, which was alluded to by Zhao *et al* in 1993 [37] and put on a firm theoretical footing by Mazin in 2000 [38], exploits the fact that CoS_2 has a Fermi level that lies low in the conduction band [35, 37–41] and that it can be alloyed with FeS_2, an isostructural diamagnetic semiconductor. This non-magnetic semiconducting behaviour arises from the $t_{2g}^6 e_g^0$ electronic configuration which gives $S = 0$, a completely filled valence band, an empty conduction band, and therefore a lower E_F [37, 38]. The solid solution $Co_{1-x}Fe_xS_2$ is then expected to have an Fe concentration (x) dependent Fermi level, implying that in a certain composition range E_F can be decreased such that it intersects the majority spin band while lying in a gap for the minority spins, producing $P = 100\%$. This situation is illustrated schematically in figure 1, which shows the crystal structures and schematic DOS diagrams for CoS_2, FeS_2 and $Co_{1-x}Fe_xS_2$. As discussed in detail in the next section, the major features of this simple picture are in fact verified by first-principles electronic structure calculations.

The $Co_{1-x}Fe_xS_2$ system therefore offers advantages over other candidate half-metals. First, we are able to deliberately 'engineer' high P by Fermi level control, as opposed to simply searching for half-metallic compounds based on the predictions of band structure calculations. Second, as pointed out by Mazin [38], the high P in this system should not be sensitive to crystallographic disorder and defects, in contrast to other systems such as Heusler alloys [19, 20, 42–44]. Third, the composition control of the spin polarization offers unique opportunities for fundamental studies of material properties as a function of P, and finally, looking forward to heterostructure fabrication, this system has a close lattice match to important semiconductors such as Si and GaAs, as well as other commercially available substrate materials (e.g. $SrTiO_3$). It has even been suggested that interfaces between CoS_2 and such semiconductors are good candidates for efficient spin filtering [45]. Although T_C is around 150 K, ruling out room-temperature applications, it seems that the $Co_{1-x}Fe_xS_2$ alloy system offers great potential opportunities for the *fundamental* study of highly spin polarized FMs and the heterostructured spintronic devices fabricated from them. This is discussed in more detail in section 10.

3. Electronic structure calculations

Several careful electronic structure calculations have been performed on the CoS_2 [35, 37–41, 46], FeS_2 [37, 38, 41, 46] and $Co_{1-x}Fe_xS_2$ [35, 38, 41, 46] systems. Although the calculations differ slightly depending on the exact computational method used, a clear consensus emerges, which verifies the simple picture shown in figure 1. In 1993 Zhao *et al* [37] used self-consistent linear combination of atomic orbitals (LCAO) calculations on pure CoS_2 and FeS_2 with the experimentally determined lattice parameters. They concluded that CoS_2 was an itinerant FM that is close to being half-metallic, i.e. the Fermi level barely cuts the spin-down DOS. They found a saturation magnetization of 0.92 μ_B/Co, the proximity to 1.0 μ_B being consistent with the small density of spin-down electrons at E_F. FeS_2 was found to be a non-FM semiconductor with a band gap (E_g) of 0.6 eV, but with a sharp increase in DOS at about 1.2 eV, consistent with experiments [37]. Zhao *et al* concluded their study by noting that, as the CoS_2 was so close to being half-metallic, 'It is plausible to suppose that the half-metallic condition might be obtained for some smaller occupation of the states in the band as would be expected in the mixed system $Fe_xCo_{1-x}S_2$'. This concept was put on a firm footing by Mazin in 2000 who performed several series of density functional theory (DFT) calculations within the local spin-density approximation (LSDA) [38]. Linearized muffin tin orbitals (LMTO) calculations were performed using both the virtual crystal approximation (VCA) (to model random alloys) and supercell (ordered alloy) approaches, and these were checked against full-potential linear augmented plane wave (FLAPW) calculations using the VCA at several compositions. CoS_2 lattice parameters were used in all cases. The CoS_2 saturation magnetization (M_S) was found to lie in the range 0.74–0.9 μ_B/Co ion, depending on the exact computational method used. Most importantly, this was found to increase with increasing Fe concentration up to 1.0 μ_B/Co at $x \approx 0.10$, this value being maintained over the large composition range out to $x \approx 0.75$. Mazin pointed out that both VCA and supercell calculations agree on half-metallicity in this wide doping range, indicating that, unlike many other proposed half-metals, the half-metallic state is insensitive to crystallographic disorder, i.e. the half-metallicity is 'robust'. It was also noted that unusual transport properties are to be expected in CoS_2 due to the strong coupling between electronic, lattice and magnetic degrees of freedom and the sharp features in the DOS near E_F. This point will be returned to in section 7.

The situation in undoped CoS_2 was further verified by Kwon *et al* [39] in 2000, who performed LMTO calculations using both LSDA and LSDA + U calculations. The LSDA approximation was found to describe CoS_2 more accurately, and it was again found that CoS_2 is close to being half-metallic, with $M_S = 0.92$ μ_B/Co. It was also shown that the minimum in the total energy occurs very close to the experimental lattice parameter. In 2001 Shishidou *et al* [40] performed FLAPW calculations using both the LSDA and generalized gradient approximation (GGA), using experimental lattice parameters. LSDA predicted close to half-metallic behaviour for CoS_2, while the GGA was found to predict a truly half-metallic state due to small changes in the e_g-derived band. As discussed in sections 5, 8 and 9, experiments are in fact not consistent with a half-metallic state for undoped CoS_2; Fe doping is required to achieve this, as suggested by Zhao *et al* [37] and Mazin [38]. Ramesha *et al* [41] also used the GGA (for LMTO calculations), concluding that, although the GGA does predict larger M_S for CoS_2, it is not truly half-metallic. Again it was found that Fe doping (using supercells and the experimental lattice parameters) leads to a half-metal over a wide doping range. This study [41] also highlighted the important role of the almost constant S–S distance in the S dimers (see next section), in that the S–S antibonding state pins E_F. Umemoto *et al* [35, 46] in 2005/2006 used LSDA pseudopotential calculations with the experimental CoS_2 lattice parameter for $x \leqslant 0.25$ and the FeS_2 lattice parameter for $x \geqslant 0.75$ in a supercell approach. It was pointed out that

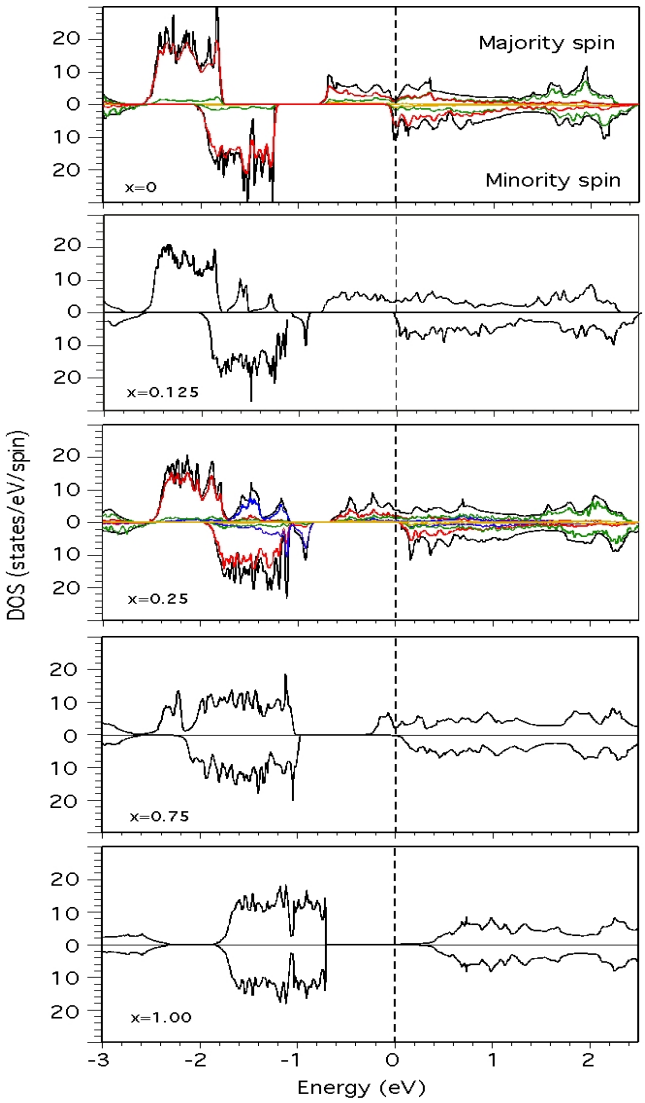

Figure 2. Calculated spin resolved density of states versus energy plots for $x = 0.00$, 0.125, 0.25, 0.75 and 1.0 (from top to bottom) from Umemoto *et al* [46] using the LSDA approximation, pseudopotentials, and supercell alloys. The zero of energy is taken as the Fermi energy. For $x = 0.00$ and 0.25, the total density of states is supplemented with the projected density of Co 3d (red), S 3s (yellow) and S 3p (green) states.

a sharp feature in the spin-down DOS near E_F for undoped CoS_2 actually leads to minority spin behaviour ($P < 0$ in our convention). Figure 2 shows their calculated DOS for $x = 0.00$, 0.125, 0.25, 0.75 and 1.0 (for the case of $x = 0.00$ and 0.25, the DOS is decomposed into Co 3d, S 3s, and S 3p states). A progression to majority spin dominance (at E_F) with doping, as seen in the prior works, therefore leads to a change in *sign* in P. Some experimental evidence for this does indeed exist (see section 7). In good agreement with prior work, the M_S increases from 0.83 to 1.00 μ_B/Co as x increases from 0.00 to 0.25. FeS_2 was again found to be a narrow-gap semiconductor, having $E_g = 0.7$ eV in this calculation. A summary of

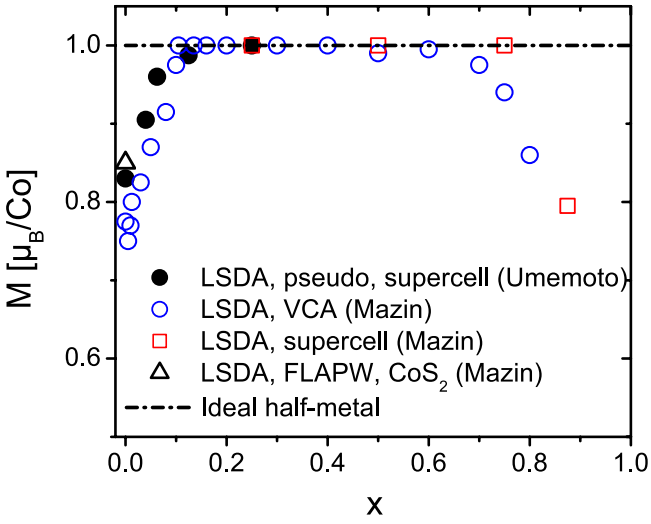

Figure 3. Fe doping concentration dependence of the theoretical saturation magnetization (in μ_B/Co ion) using various computational tools: solid black circles are from LSDA pseudopotential supercell calculations (Umemoto *et al* [35, 46]); open circles are from LSDA LMTO virtual crystal approximation calculations (Mazin *et al* [38]); open squares are from LSDA LMTO supercell calculations (Mazin *et al* [38]); and the open black triangle is an LSDA FLAPW calculation for pure CoS_2 [38].

the Fe doping dependence of M_S is given in figure 3, showing the Mazin [38] and Umemoto *et al* [35, 46] results. The broad composition range over which half-metallicity is predicted is clear.

Finally, it is worth pointing out that, according to the theoretical considerations of Kirczenow [45], CoS_2 is a good candidate for an efficient spin filtering effect when used as a contact to zincblende or diamond semiconductors. This implies that spin filtering could be used to further enhance the intrinsically high P in lightly doped $Co_{1-x}Fe_xS_2$ to inject highly spin polarized currents into closely lattice matched non-magnetic semiconductors such as Si and GaAs. This will be returned to in section 10.

4. Structure and synthesis

A schematic illustration of the crystal structure of CoS_2 and FeS_2 is shown in figure 1. The structure is of Pyrite type (space group no. 205, $Pa\bar{3}$) with four Co atoms (at (0, 0, 0) and equivalent positions) and eight S atoms (at (u, u, u), $(u = 0.39)$ and equivalent positions) in the unit cell. Essentially, the Pyrite structure has a face-centred cubic (fcc) arrangement of metal ions bonded to a set of S dimers. The valence states of the end members are therefore $Co^{2+}(S_2)^{2-}$ and $Fe^{2+}(S_2)^{2-}$ and the dominant crystal field splitting leads to electronic configurations of $t_{2g}^6e_g^1$ ($S = 1/2$, low spin) and $t_{2g}^6e_g^0$ ($S = 0$, low spin), giving rise to their respective behaviours as FM metal and diamagnetic semiconductor. The importance of the S–S dimers in dictating the electronic structure and the half-metallicity of the intermediate alloys was discussed by Ramesha *et al* [41]. The lattice parameter, a, is 5.53 and 5.41 Å for CoS_2 and FeS_2, respectively. Solid solutions are obtained over the whole composition range, as expected. Figure 4 shows the Fe doping dependence of the lattice parameter from a variety of studies on both polycrystals and single crystals [35, 41, 47–49]. The overall agreement is good.

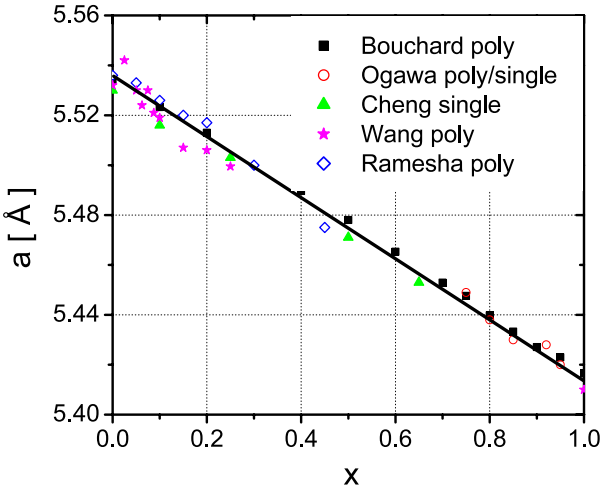

Figure 4. Fe doping concentration dependence of the cubic lattice parameter (a) of $Co_{1-x}Fe_xS_2$ taken from various experimental works (polycrystals by coprecipitation (Bouchard *et al* [47]), polycrystals by coprecipitation and single crystals by iodine vapour transport (Ogawa *et al* [48]), single crystals by temperature gradient solution growth with a Te flux (Cheng *et al* [49]), polycrystals by high-temperature solid-state reaction with resulfurization (Wang *et al* [35, 64])) and polycrystals by low-temperature solid-state reaction (Ramesha *et al* [41]). The solid line is a fit to Vegard's law for substitutional solid solutions. See the individual references for exact experimental conditions and sample fabrication details.

As noted by Bouchard [47], the fabrication of polycrystalline samples by solid-state reaction is difficult, but successful reports exist for $Co_{1-x}Fe_xS_2$ by low-temperature solid-state reaction [41] and high-temperature solid-state reaction with resulfurization [35]. Examination of the Co–S phase diagram reveals two other line compounds that are stable at room temperature (Co_9S_8 and Co_3S_4). The major difficulty in the preparation of CoS_2 and $Co_{1-x}Fe_xS_2$, however, is the loss of S at higher temperatures. As stated above, this can be avoided either by the use of low temperatures (not ideal from the diffusion point of view) or by high-temperature processing followed by resulfurization at low T [35]. This resulfurization likely relies on grain boundary diffusion, and will therefore only be effective for thin films and polycrystals. Co-precipitation has also been used [47, 48].

Successful single-crystal growth has been reported by vapour transport using both chlorine [50, 51] and iodine [48, 52, 53] transport gases. The use of a $CoBr_2$ flux [54, 55] or temperature gradient solution growth with a Te flux [49] have both been effective. Chemical vapour transport using $CoBr_2$ has also been reported for single-crystal CoS_2 [56], as shown in figure 5, which summarizes the structural characterization of such a sample. Figures 5(a) and (b) show the wide-angle x-ray diffraction patterns from a powdered crystal and a (100) oriented crystal, while 5(c) shows that the full-width at half-maximum of the rocking curve through the (200) peak is only 0.004° (resolution limited in this case). Single crystals of high crystalline quality can therefore be fabricated and, as shown in figure 5(d), typical sizes are of the order of a few millimetres. In addition to diffraction characterization, energy dispersive spectroscopy (EDS) and inductively coupled plasma optical emission spectroscopy (ICPOES) are often used as probes of S stoichiometry. This stoichiometry varies significantly, depending on the exact synthesis method and conditions. For instance, Te flux growth [49] resulted in 1.5–10% S deficiency and significant incorporation of Te impurities, while chemical vapour

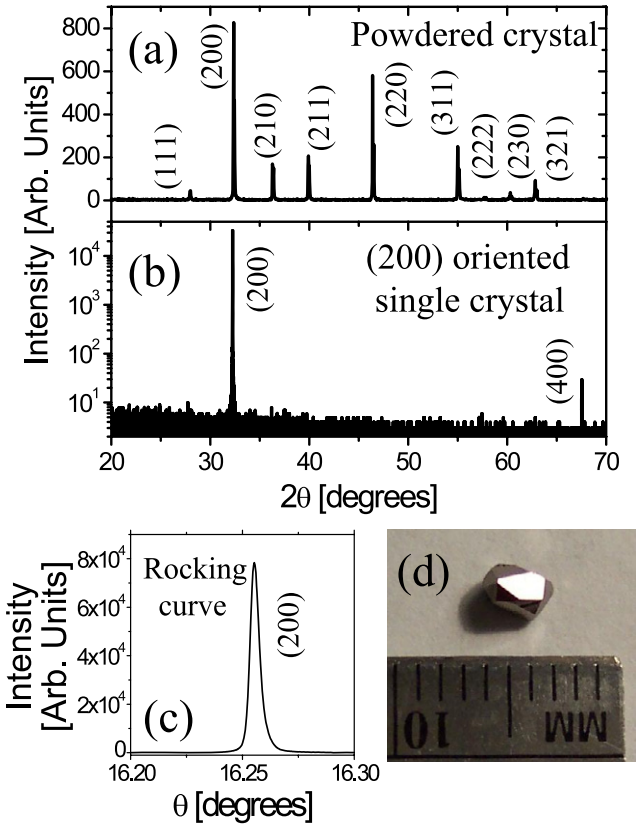

Figure 5. Summary of structural characterization of a CoS_2 single crystal grown by the chemical vapour transport method [56]: (a) shows the wide-angle x-ray diffraction pattern from a powdered single crystal; (b) shows the wide-angle x-ray diffraction from a bulk crystal oriented with the scattering vector perpendicular to the (100) family of planes; (c) shows the 'rocking curve' or transverse scan through the (200) diffraction peak; (d) is a photograph of a typical crystal. See the reference for exact experimental conditions and sample fabrication details.

transport resulted in finely controlled stoichiometry. Wang *et al* [56] measured the EDS S content, rocking curve width, T_C, residual resistivity, residual resistivity ratio (RRR), and low-T positive magnetoresistance (MR) as a function of S mass used in the chemical vapour transport growth. A minimum in the rocking curve width and residual resistivity accompanied a sharp peak in RRR and low-T MR at a S concentration near 66.6 at.%, demonstrating good stoichiometry control. As discussed in section 10, the S content has been found to have a significant effect on P.

As mentioned above, $Co_{1-x}Fe_xS_2$ alloys offer great opportunities for the fabrication of unique heterostructures where the tunability in P is exploited, and it is therefore important to consider thin-film growth. Although little work has been done on CoS_2 films, a significant literature on FeS_2 films exists, primarily due to potential solar cell applications. Reactive sputtering from a sulfide target in the presence of S gas [57], reactive sputtering from sulfide or elemental targets using an Ar/H_2S plasma [58], metal–organic chemical vapour deposition (MOCVD) [59], molecular beam deposition [60], and sulfidization of pre-deposited metal films [61–63] have all been used. Thin-film heterostructure possibilities will be discussed in more detail in section 10.

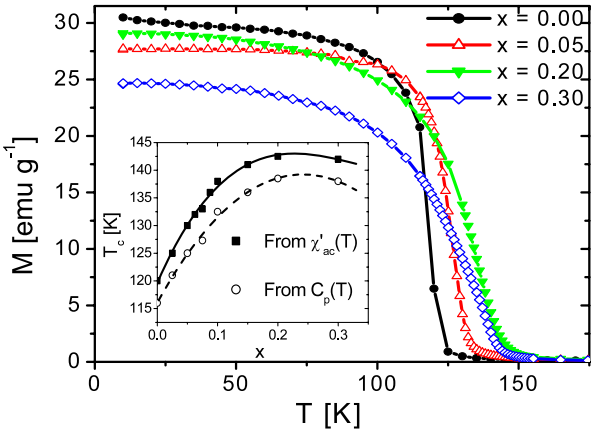

Figure 6. Temperature dependence of the dc magnetization of $x = 0.00$, 0.05, 0.20 and 0.30 in a static 1 kOe field. Inset: Fe doping concentration dependence of the Curie temperature determined by both ac susceptibility (solid squares) and heat capacity (open circles). All data are on polycrystalline samples from Wang *et al* [35, 64]. See the reference for exact experimental conditions and sample fabrication details.

5. Basic magnetic properties

The basic magnetic properties of $Co_{1-x}Fe_xS_2$ alloys (low Fe content) are illustrated in figure 6, which shows the T dependence of the magnetization of $x = 0.00$, 0.05, 0.20 and 0.30 polycrystals (Wang *et al* [64]) measured in a 1 kOe field. Undoped CoS_2 shows a sharp FM to paramagnetic (P) phase transition at a T_C of approximately 120 K. Two observations can be made as x increases: (i) T_C increases, up to ∼145 K at $x = 0.20$, and (ii) the sharp transition that occurs at $x = 0.0$ is broadened with increasing x. The latter observation is due to the fact that undoped CoS_2 lies close to a tricritical point separating a first-order FM → P transition from a conventional second-order FM → P transition [36, 64, 65]. The transition apparently becomes second order as doping increases. The increase in T_C with increasing doping is intriguing in light of the fact that the Fe ions are expected to be non-magnetic (FeS_2 has electronic configuration $t_{2g}^6 e_g^0$, $S = 0$), implying that the T_C is enhanced by dilution with non-magnetic impurities. This simple argument is shown to be valid in the next section, where element-resolved magnetometry reveals essentially zero moment on the Fe site. Although the mechanism for the T_C enhancement is not understood (it could be related to the increase in M_S/Co ion, discussed below) it is interesting to note that disorder-induced enhancements in T_C can be found in the dynamical mean-field treatment of the disordered one-band Hubbard model [66].

A clear variation in M_S with Fe doping is also seen in figure 6. As discussed in section 3 on electronic structure, measurement of the M_S per Co ion provides an important probe of the potential half-metallic state in $Co_{1-x}Fe_xS_2$. The determination of M_S in μ_B/Co ion requires the assumption of zero moment on the Fe sites, which, as we just mentioned, will be verified by element-resolved magnetometry in the next section. Figure 7 shows the Fe doping dependence of M_S from multiple studies on both polycrystalline and single-crystal specimens [35, 41, 48, 67]. Starting at $x = 0.0$, M_S increases rapidly from 0.83 to 0.92 μ_B/Co, reaching the predicted value of 1.0 μ_B/Co at $x \approx 0.10$. The ideal value is maintained out to $x \approx 0.5$–0.6, where it decreases again. Although there is considerable scatter of the points in figure 7, it must be stressed that careful individual studies on single series of well-characterized

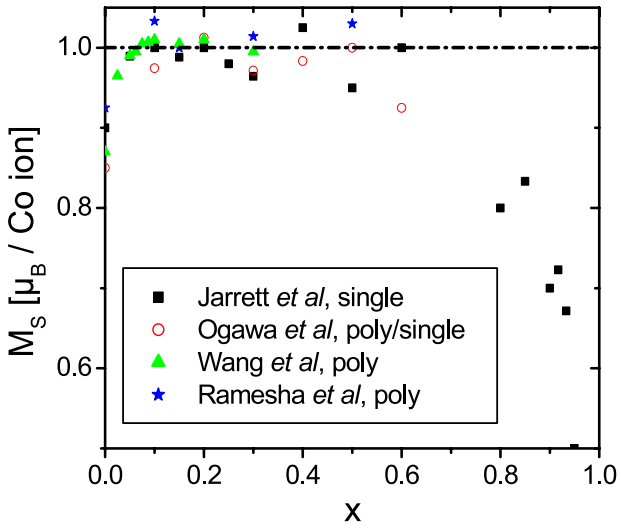

Figure 7. Fe doping dependence of the saturation magnetization per Co ion (assuming zero moment on the Fe sites) from four separate studies: Jarret *et al* [67], Ogawa *et al* [48], Wang *et al* [35, 64], and Ramesha *et al* [41]. See the individual references for exact experimental conditions and sample details.

samples (e.g. the data of Wang *et al* [35]) show consistent behaviour, with an M_S of 1.0 μ_B/Co being attained at $x = 0.07$.

Compared to the prediction of electronic structure calculations in figure 3, we see that the range over which ideal magnetization occurs may be slightly smaller than predicted, but the overall agreement is good. These data are therefore consistent with a half-metallic state at $x > 0.07$. It is important to note that achieving an M_S of an integer number of Bohr magnetons per Co ion is a necessary but not sufficient condition for half-metallicity. Further evidence of a highly polarized state requires more direct probes of P.

Other important aspects of the basic magnetic behaviour have also been investigated in CoS_2 and $Co_{1-x}Fe_xS_2$. The critical behaviour of CoS_2 has attracted some attention due to the aforementioned proximity to a tricritical point. Magnetization, susceptibility, heat capacity, and neutron scattering have been used to probe the region near T_C, confirming the almost first-order nature of the FM $\rightarrow$ P transition [65]. Angle-dependent hysteresis loop measurements have also been made [65]. They reveal low coercivity and low saturation fields (<300 Oe at 4.2 K), the [111] directions being the easy axes. The [111] easy axis was confirmed by torque magnetometry measurements [55] that determined a low-T cubic magnetocrystalline anisotropy of only 2.5×10^4 erg cm^{-3}. This anisotropy is sufficiently low that CoS_2 can be considered to be essentially isotropic, consistent with the negligible gap found in the spin wave dispersion relation from inelastic neutron scattering [68]. FM nuclear magnetic resonance (NMR) measurements have been made as a function of Fe doping, as discussed in more detail in section 9.

6. Element-resolved magnetometry (x-ray magnetic circular dichroism studies)

The determination of the Fe doping dependence of the M_S per Co ion requires the assumption that the magnetic moment is confined to the Co sites, i.e. that the moment on the Fe atoms is small, as suggested by simple crystal field arguments. In a real itinerant FM this assumption must be validated experimentally. The well-established x-ray magnetic circular

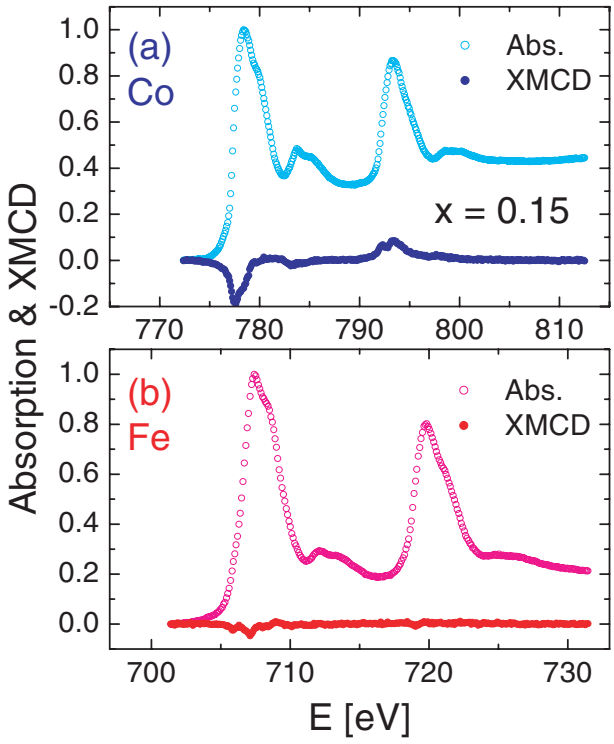

Figure 8. X-ray absorption spectroscopy and XMCD measured by fluorescence yield on $Co_{0.85}Fe_{0.15}S_2$ single crystals while scanning the incident x-ray energy through (a) the Co L-edge and (b) the Fe L-edge. The data were taken in zero field at 30 K after cooling in 500 Oe.

dichroism (XMCD) technique [2] is ideally suited to this task. XMCD employs energy tunable synchrotron radiation to achieve resonant absorption specific to individual atomic species, i.e. it is chemically selective. These element specific absorption lines display differences in intensity for left and right circularly polarized photons in the case when a net magnetic moment exists on that specific atomic site. For the measurements presented here, this absorption was detected using the 'total fluorescence yield', which probes to depths of order 10–100 nm, i.e. relatively deep. Figure 8 shows the absorption and XMCD signals at the Co and Fe L-edges for an $x = 0.15$ $Co_{1-x}Fe_xS_2$ single crystal. The data were taken at beamline 4-ID-C of the advanced photon source at Argonne National Laboratory using crystals grown by the chemical vapour transport method at the University of Minnesota. Both the Co and Fe absorptions are clearly observed (776, 792 eV and 707, 719 eV, respectively) but the data reveal a large XMCD signal only for the case of Co. This demonstrates directly that the vast majority of the magnetic moment in $Co_{0.85}Fe_{0.15}S_2$ resides on the Co sites, validating the prior assumptions. The fact that this conclusion holds at other Fe dopings is demonstrated by figure 9, which shows the XMCD signal for $x = 0.10$ and 0.15 single crystals. Again, no large XMCD is observed at the Fe edge, even up to compositions at which an M_S of 1.0 μ_B/Co has already been attained. If we make the assumption that the size of the Co and Fe XMCD signals can be directly compared, then we estimate that the Fe moment contributes ~0.03 μ_B to the total saturation magnetization at $x = 0.15$. In principle, quantitative analysis of these data can be performed to not only determine the precise Co moment and place an upper bound on the Fe moment, but also to decompose the Co moment into orbital and spin components. This will be explored in future work.

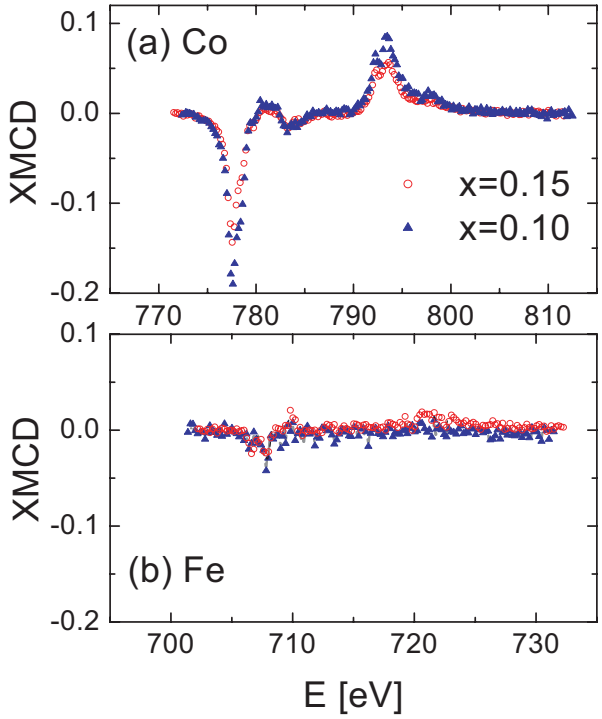

Figure 9. XMCD (fluorescence yield) on $Co_{1-x}Fe_xS_2$ single crystals ($x = 0.10$ and 0.15) measured while scanning the incident x-ray energy through (a) the Co L-edge and (b) the Fe L-edge. The data were taken in zero field at 30 K after cooling in a Oe field.

7. Electronic transport properties

As discussed in section 3, there are numerous reasons to anticipate unusual transport phenomena in the $Co_{1-x}Fe_xS_2$ system. The temperature-dependent resistivity (ρ) and conductivity (σ) data of figure 10 (polycrystals—Wang *et al* [35, 64]) confirm that this is indeed true. Undoped CoS_2 already provides some interesting behaviour; $\rho(T)$ is metallic-like (i.e. $d\rho/dT > 0$) both at $T > T_C$ and at $T \ll T_C$, but as T is lowered below T_C the resistivity shows a sharp increase (∼7%), as discussed in several prior works [36, 52, 53]. Ogawa *et al* [52] argued that the magnitude and form of this anomaly were inconsistent with conventional critical scattering, and Wang *et al* [36] proposed that this is actually a spin-dependent band structure effect. The basic concept is that the exchange splitting that sets in when the sample is cooled through T_C leads to a sharp decrease in the spin-averaged DOS at E_F due to the fact that the DOS in the FM state is derived primarily from only one spin orientation. The aforementioned proximity to a first-order FM → P phase transition means that the application of large magnetic fields at temperatures just above T_C leads to entry to the FM state and therefore a positive MR effect of equal magnitude to that seen on cooling (i.e. 7%). In essence, the resistivity near T_C is controlled by the magnetization, regardless of whether the P → FM transition is driven by cooling or field application. At lower temperature (e.g. $T \approx T_C/2$) a negative contribution to the MR is dominant, due to the field-induced suppression of electron-magnon scattering, as is the case in any conventional FM. At still lower T (e.g. 5 K) a large positive MR prevails, increasing with decreasing T, as is typically the case in metals.

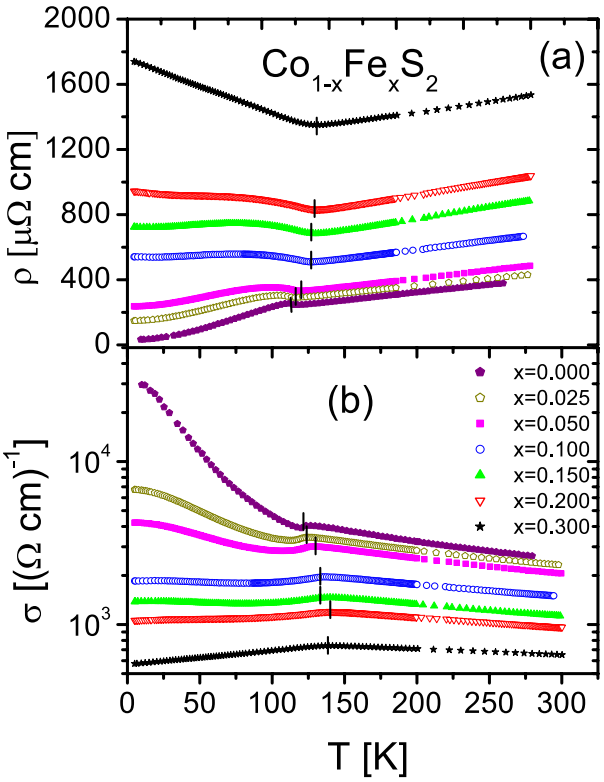

Figure 10. Zero magnetic field temperature dependence of (a) the resistivity and (b) the conductivity for $x = 0.000$, 0.025, 0.050, 0.100, 0.150, 0.200, and 0.300. The short vertical lines indicate the position of T_C. Data from [64]. See reference for details on exact experimental conditions and sample details.

Let us now turn to the Fe-doped case. As seen in figure 10, the overall trend is to higher ρ with increasing x, as expected (FeS_2 is a semiconductor). The evolution of $\rho(T)$ with increasing x is intriguing and is discussed in more detail in [64]. At $T > T_C$ the resistivity is still metallic-like, but the behaviour below T_C is complex. The $T = 0$ value of $d\rho/dT$ changes sign with increasing x, meaning that, for $x > 0.10$, $d\rho/dT$ actually changes sign at T_C. Metallic-like temperature dependences are observed above T_C, changing to insulating-like temperature dependences below T_C, which is opposite to what is observed in many other FM systems. The linear $\rho(T)$ at $T < T_C$ for high x (e.g. $x = 0.30$) is also remarkable. The data can be interpreted qualitatively in terms of the relative positions of the mobility edge (E_μ) and E_F, although a quantitative description is lacking. The essential concept is that the exchange splitting that occurs on cooling below T_C leads to a situation where only a single spin band contributes to the transport. As x increases, E_F is lowered, eventually to the point where it falls below E_μ. A positive MR in the vicinity of T_C is observed at all x up to 0.3, again due to the fact that the resistivity is controlled by the magnetization.

In terms of further evidence for a highly polarized state with increasing x, the negative MR below T_C (due to the suppression of electron–magnon scattering) is of particular interest. As shown in figure 11(a), the magnitude of this effect decreases rapidly from ~10% at $x = 0$ to essentially zero at $x = 0.07$, i.e. the same composition that attains $M_S = 1.0\ \mu_B$/Co.

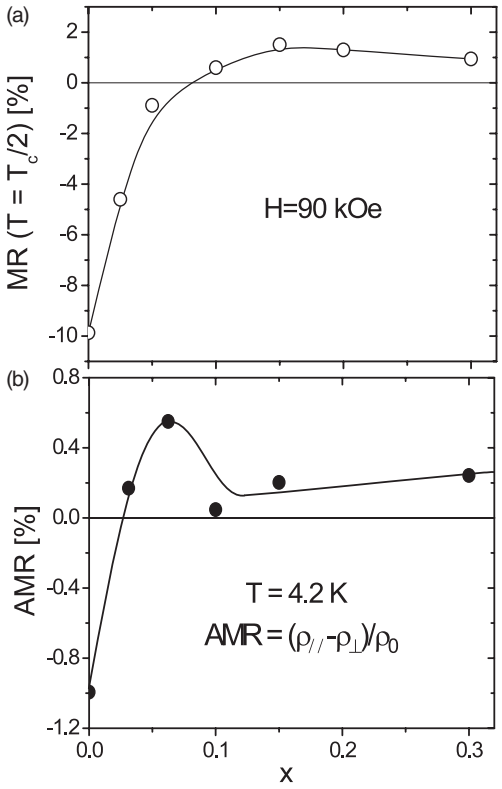

Figure 11. Fe doping dependence of (a) the 90 kOe MR at $T_C/2$ (this temperature was chosen as representative of the region where the negative MR dominates), and (b) the AMR ratio (defined in the figure) at $T = 4.2$ K and $H = 80$ kOe. Data from [35, 64]. See reference for exact experimental conditions and sample details.

Wang *et al* [35] interpreted this as further evidence for a highly polarized state at $x > 0.07$, arguing that the absence of minority spin states eliminates electron–magnon spin flip scattering, leading to zero MR. The small positive MR at $x > 0.07$ in figure 11(a) is a remnant from the aforementioned positive component near T_C.

The anisotropic magnetoresistance (AMR) is also a useful probe of P, as some of the original theoretical work on AMR [69] predicted that the sign of the AMR (i.e. the relative magnitude of ρ when the magnetization and current are perpendicular or parallel) reflects the sign of P (i.e. majority or minority spin). This is of particular importance here, as the calculations of Umemoto *et al* [35, 46] predict a sign reversal in P with increasing x, and the PCAR technique is insensitive to the sign of P. Figure 11(b) shows that the AMR ($T = 4.2$ K) does indeed change sign between $x = 0$ and 0.03. Note that the point at $x = 0$, which shows a very typical AMR of about 1%, is actually the average of three separate samples, each of which showed negative values. Following McGuire and Potter [69], we interpret this reversal in sign of the AMR as a reversal in sign of P, meaning that we are observing a crossover from minority to majority dominance at $x = 0.03$, prior to attaining 1.0 μ_B/Co and zero spin-flip scattering contribution to the resistivity at $x = 0.07$. Aside from the disagreement regarding the exact x values at which these transitions occur, these data are therefore in good agreement with the predictions of Umemoto *et al* [35, 46].

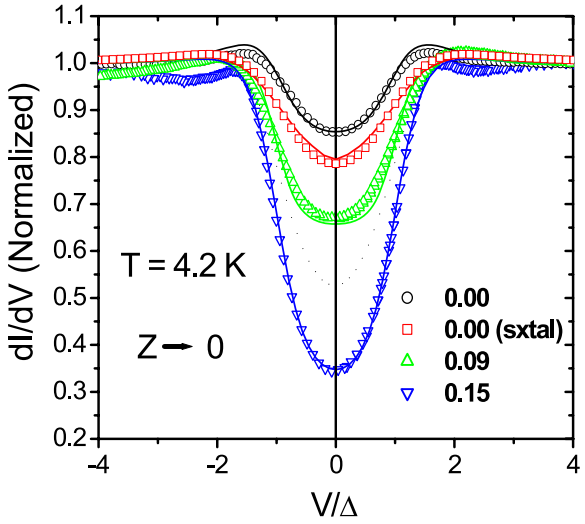

Figure 12. PCAR conductance–voltage curves for $x = 0.00$ (both polycrystal and single crystal), 0.09, and 0.15 at 4.2 K in zero magnetic field. The conductance is normalized to the normal state value (at a voltage of $+4.0$ V/Δ), while the voltage is normalized to the superconducting gap voltage, Δ. The solid lines are fits to the model described in the text with fitting parameters: $x = 0.00$ (poly), $P = 57\%$, $Z = 0.00$; $x = 0.00$ (single), $P = 63\%$, $Z = 0.00$; $x = 0.09$, $P = 56\%$, $Z = 0.08$; $x = 0.15$, $P = 80\%$, $Z = 0.28$. Taken from [35, 56, 64]. See reference for exact experimental conditions and sample details.

8. Direct experimental probes of the transport spin polarization

As discussed in section 1, spin-resolved photoemission, PCAR, planar Andréev reflection, Meservey–Tedrow tunnelling into a superconducting electrode, and FM/insulator/FM tunnelling are all valuable probes of P, albeit with differing definitions applying to different techniques. Of these methods, only PCAR has been applied to CoS_2 and $Co_{1-x}Fe_xS_2$. Cheng *et al* [49] used Sn tips at 1.5 K to probe the conduction electron polarization of $Co_{1-x}Fe_xS_2$ single crystals ($0.00 < x < 0.65$) grown by the temperature gradient solution growth method, and having 1.5 to 10% S deficiency. They observed P values of order 50%, with a very weak dependence on x. They attributed the low P, and the disparity between the experiments and the calculation results discussed in section 3, to the S non-stoichiometry, pointing out that this once again highlights the importance of stoichiometry for half-metallic materials. Wang *et al* [35, 36, 56, 64] used Pb and NbN superconducting tips to perform PCAR at 4.2 K on stoichiometric polycrystals ($0.00 < x < 0.30$). Figure 12 shows the evolution with composition of the conductance, G (normalized to the normal state conductance), as a function of the bias voltage, V (normalized to the superconducting gap voltage). The data reveal a rapid decrease in zero-bias conductance with increasing doping up to $x = 0.15$; these $V = 0$ conductance values suggesting (via the simplest possible analysis [13, 14]) polarizations of 58, 66 and 83% for $x = 0.00$, 0.09 and 0.15, respectively. Full fits to the model of [70] provide P values of 57, 56 and 80% at $x = 0.00$, 0.09, and 0.15, respectively, with the full fitting parameters given in the caption. Note that the data of figure 12 correspond to the smallest Z values measured in each case (0.00, 0.08 and 0.28, respectively), where Z is the dimensionless number parametrizing the interface barrier strength. Measuring multiple point contacts and plotting P as a function of Z, then extrapolating to $Z = 0$, gives P values of 57, 67 and 85% for $x = 0.00$, 0.09 and 0.15, respectively, little different from the simple model discussed above.

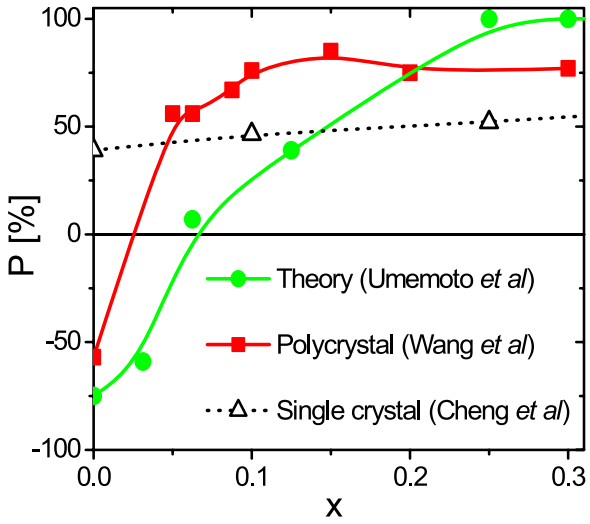

Figure 13. Fe doping concentration dependence of the absolute spin polarization from theory (Umemoto *et al* [35, 46], LSDA calculations) and experiments (Wang *et al* [35, 64] stoichiometric polycrystals and Cheng *et al* [49] S-deficient single crystals). For the data of Wang *et al*, the negative value at $x = 0$ has the sign determined by AMR and is actually based on three separate samples. See the individual references for exact experimental conditions and details on sample preparation.

The doping dependence of the $Z = 0$ values of PCAR spin polarization from the Wang *et al* study of stoichiometric polycrystals [35, 64] is shown in figure 13, along with the theoretical result of Umemoto *et al* [35, 64] and the data of Cheng *et al* [49] on S-deficient single crystals. In this figure the $x = 0.00$ point of Wang *et al* is shown as negative (i.e. minority spin) due to the conclusions from the AMR experiments discussed above. It is clear from this figure that (i) the S deficiency provides a significant problem, and (ii) the overall agreement between electronic structure calculations and experiments on stoichiometric samples is good, at least qualitatively. Evidence exists for the predicted sign reversal (this comes only from AMR, as PCAR is insensitive to the sign of P) and, most importantly, large majority spin polarizations are observed above a certain Fe doping concentration. Although the qualitative agreement is good, there are several points of quantitative disagreement between experiment and theory, namely regarding: (i) the x value at which the sign reversal takes place; (ii) the x value at which P saturates at the largest majority value; and (iii) the maximum P observed. Of these, the latter is obviously the most important. PCAR on stoichiometric polycrystals results in maximum observed P of 85% compared to the 100% predicted universally by first-principles electronic structure calculations, regardless of the details of the computational method used (see prior comments in section 3). There are various possible origins for this discrepancy. First, as pointed out in section 1, it is hazardous to compare polarization of the transport current from PCAR measurements (which are weighted with the spin-dependent v_F) directly with calculated DOS polarizations. Although future theoretical work on the x dependence of $v_{F\uparrow,\downarrow}$ should be encouraged, it obviously cannot completely resolve the discrepancy between theory and experiment, as the $P = 100\%$ prediction will be unaffected. Second, it is important to point out that the alloys used in experiment appear to be random, while many of the calculations are baed on the use of supercells, i.e. they model ordered alloys. As pointed out by Mazin [38], the VCA and supercell approaches both predict a HMF state for $Co_{1-x}Fe_xS_2$, suggesting that this is not likely to be a major factor. Note from figure 3 that LSDA calculations within the VCA

show an onset of maximum polarization at lower x than the supercell calculations, in closer agreement with the experimental value of $x = 0.07$–0.15. Mazin also outlined the arguments for insensitivity of the spin polarization of this system to crystallographic disorder, based on the similarity between the supercell and VCA results. The experiments on S-deficient single crystals certainly indicate that the S *stoichiometry* remains of vital importance. Generally, there is little understanding about the influence of other point defects or grain boundaries in this material. PCAR data from a stoichiometric single crystal [56] of CoS_2 ($x = 0.00$) are also shown in figure 12 to compare with the polycrystals. The crystals show low Z spin polarization of 65%, which is a significant increase over the 56% observed in polycrystals [36]. This will be returned to in section 10, although it should be noted that it is unclear whether this improvement is due to the absence of grain boundaries, improvements in S stoichiometry, or improved structure/stoichiometry at the surface region. Finally, it is important to note that the superconductor/FM interface is poorly controlled in PCAR experiments and cannot be subject to the usual structural characterization. It is important that other measurement types such as photoemission, planar Andréev reflection, and Meservey–Tedrow tunnelling are applied to these materials. These measurements will likely require single-crystal samples with sufficiently large facets.

In summary, the measurements available to date do indicate very high spin polarization at low temperature, the value of 85% being bettered only by CrO_2 and lying very close to $Ga_{1-x}Mn_xAs$, $La_{1-x}Sr_xMnO_3$ and Fe_3O_4 results. In addition, the tunability in P is an attractive feature, which could offer unique opportunities for fundamental studies of spintronic devices, as discussed in section 10. The 85% polarizations do fall short of the half-metallic predictions though, and this will be discussed further in section 10.

9. Experimental probes of the total density of states

In addition to the PCAR measurements designed to probe the spin-dependent DOS there have also been two investigations on $Co_{1-x}Fe_xS_2$ polycrystals designed to probe the total DOS at E_F, i.e. $[N_\uparrow(E_F)+N_\downarrow(E_F)]$. The first (see [64] and [71]) involves measuring the T dependence of the specific heat and extracting the total DOS from the electronic contribution evident at low T. The specific heat, $C_P(T)$, was found to follow $C_P(T) = \gamma T + \beta T^3$ at low T, where γ, the electronic contribution, is given by $\gamma = \pi^2 k_B^2[N_\uparrow(E_F)+N_\downarrow(E_F)]/2$ within the free electron gas model, and the second term is due to the lattice (phonon) contribution. Note the absence of a spin wave contribution, which was not required to describe the data, although a strong magnetic peak was observed at T_C. The results for the total DOS extracted from such measurements are shown in figure 14, along with the calculations of Umemoto *et al* [35, 46, 71] for comparison. This figure also includes the results from the low-field ^{59}Co NMR measurements of Kuhns *et al* [71]. The NMR method involves the development of a theory (specific to $Co_{1-x}Fe_xS_2$, although it could be generalized to other highly polarized magnets) for the Co spin–lattice relaxation rate. This rate was found to follow the form $1/T_1 = C[N_\uparrow^2(E_F) + N_\downarrow^2(E_F)]T$, where T_1 is the Co spin lattice relaxation time, and C is a constant. This Korringa-like T dependence was indeed observed in experiments and allowed for an extraction of the total DOS after (the non-trivial) calculation of the constant C. The data are shown in figure 14, showing a remarkable agreement with those from the independent heat capacity measurements. The agreement between experiments and theory is less perfect, although it remains impressive given the absence of any adjustable parameters. The overall trend of decreasing DOS with increasing doping is due to the elimination of any contribution to the DOS at E_F from the minority spin channel (as $P \to 100\%$), leading to an approximately two-fold decrease from $x = 0.00$ to 0.10. The flattening in $N(E_F)$ versus x at $x \approx 0.10$ in the experiments is consistent with the onset

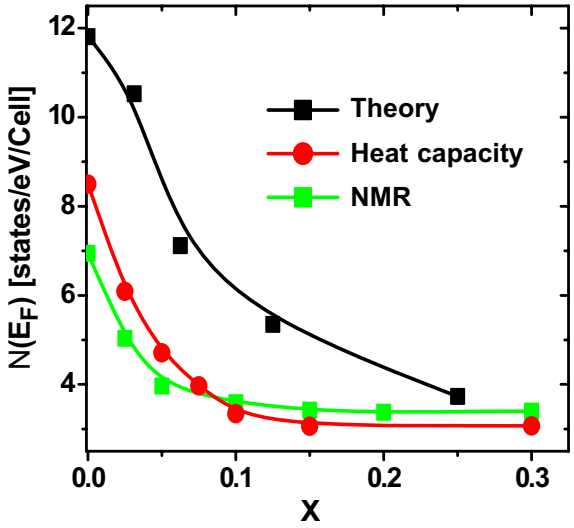

Figure 14. Total (both spin channels) density of states at the Fermi level as a function of the Fe doping concentration from theory (Umemoto *et al* [35, 46], LSDA calculations) and experiment (Wang *et al* [35, 64] polycrystals). The experimental values are extracted from heat capacity (Wang *et al* [64]) and the spin–lattice relaxation rates from ^{59}Co NMR (Kuhns *et al* [71]). See the individual references for exact experimental conditions and sample fabrication details.

of ideal M_S values, the absence of spin-flip scattering, and high P (see figures 7, 11 and 13). Moreover, the results clearly indicate that the theoretical picture shown in figures 1–3 is indeed correct, i.e. we understand in considerable detail the evolution of the electronic structure of $Co_{1-x}Fe_xS_2$ with doping.

10. Factors influencing/limiting the spin polarization, and outlook

It is clear from figure 3 that electronic band structure calculations made using multiple methods are all in agreement, as is the simple physical picture of figure 1, that a state with $P = 100\%$ should be achieved over a wide doping range in $Co_{1-x}Fe_xS_2$. Experiments reveal spin polarizations of 85% at most, which, although high, fall short of the expectations of half-metallic behaviour. It is therefore important, both for the understanding of the current data and for the motivation of future work, to identify possible mechanisms that influence or even limit the experimentally achievable P. First, as shown by figure 13, the control of S stoichiometry is clearly an important issue. Although fine control over the stoichiometry has been claimed in CoS_2 single crystals using a variety of characterization techniques, this has not been convincingly demonstrated in Fe-doped single crystals. This is an important area for future work. Currently, there has been no single well-controlled study of P as a function of S stoichiometry (varied over a wide range) at any Fe doping level. Second, the effect of the presence of other forms of structural imperfections and disorder, such as point defects, grain boundaries, and possible chemical segregation in the surface region, are unknown. Nominally stoichiometric CoS_2 single crystals seem to have higher polarizations (65% cf 56%) than nominally stoichiometric polycrystals, but the exact origin of this enhancement (and its Fe doping dependence) is unknown. Progress in this area will require that detailed atomic-level structural characterization is performed, and that the results of that work are properly correlated with accurate spin polarization measurements by multiple techniques. The use of multiple

techniques to probe P is important. The major technique applied to $Co_{1-x}Fe_xS_2$ thus far (i.e. PCAR) suffers from a poorly controlled interface, unlike some other techniques such as planar Andréev reflection, the Meservey–Tedrow superconducting tunnelling method, and spin-resolved photoemission. Application of these techniques will likely require synthesis (as well as detailed structural and chemical characterization) of $Co_{1-x}Fe_xS_2$ single crystals with sufficiently large facets to enable the measurements. Such studies should be highly revealing. They will allow us to determine the intrinsic limits on the spin polarization in this system, i.e. whether the enhancement seen on going from polycrystalline to single-crystal samples at $x = 0$ is preserved at $x = 0.15$. If it is, then can we achieve full polarization, i.e. a truly half-metallic state at low T? The temperature dependence of P is another important issue that has been neglected thus far in these materials. There is now a significant body of evidence, from both theory and experiment, that many highly polarized systems show decreases in P with increasing T due to various effects, including excitation of magnons [32–34, 72]. This is an open issue for the sulfides. Although techniques relying on superconducting electrodes cannot be applied at higher T, photoemission and indirect probes such as the transport methods described earlier (e.g. figure 11(a)) could shed further light on the T dependence of P.

Finally, it is clear from these results that $Co_{1-x}Fe_xS_2$ provides some very exciting opportunities for fundamental research on spintronic devices if it can be synthesized in the form of high-quality thin films and integrated into heterostructures. The use of a FM electrode with a tunable P would enable the study of device performance as a controlled function of the electrode spin polarization. This is particularly appealing given the close lattice match to technologically important semiconductors such as GaAs and Si, as well as other commercially available single-crystal substrate materials such as $SrTiO_3$. We envisage example devices such as $Co_{1-x}Fe_xS_2$ tunable spin injectors on GaAs-based quantum well structures to enable measurements of spin injection efficiency as a function of injector polarization. Moreover, there exist other transition-metal disulfides with similar chemistry and lattice parameter but widely varying physical properties, allowing us to speculate that the growth of all sulfide heterostructures with exciting functions is possible. As an example, CuS_2 is a non-magnetic metal that has been reported to be superconducting at low temperatures [67]. $Co_{1-x}Fe_xS_2/CuS_2/Co_{1-x}Fe_xS_2$ trilayers would then allow for study of a tunable spin valve system, while $Co_{1-x}Fe_xS_2/CuS_2$ bilayers at low temperature would allow for a planar Andréev reflection measurement in a lattice-matched epitaxial bilayer. Although little work has been done on the fabrication and characterization of CoS_2-based thin films and heterostructures, the initial work can be guided by the considerable literature on FeS_2 films [57–63], which was primarily motivated by solar cell applications.

11. Summary and conclusions

The current theoretical and experimental understanding of $Co_{1-x}Fe_xS_2$ establishes unequivocally that this material has a high (up to 85%) low-temperature conduction electron spin polarization which is tunable via composition. This system therefore offers some unique opportunities, both for studies of magnetic, transport, and thermodynamic properties as a function of spin polarization, and also as a component in thin-film heterostructures for fundamental investigations of spintronic device function. Stoichiometric materials have been synthesized in both polycrystalline and single-crystal form and have been subjected to a wide variety of direct and indirect probes of the electronic structure and spin polarization at the Fermi edge. The theoretical and experimental data provide a consistent picture of the situation, where the position of the Fermi energy with respect to the spin split bands can be fine tuned by alloying, in essence applying the concept of band engineering to half-metallic ferromagnets.

Important areas for future work, and exciting opportunities for future scientific investigations, have been discussed.

Acknowledgments

Work at the University of Minnesota was supported by the US National Science Foundation (NSF) Materials Research Science and Engineering Center (MRSEC) program. Use of the Advanced Photon Source is supported by the US Department of Energy (DoE) Office of Science under contract DE-AC02-06CH11357. RMW and KU acknowledge support from NSF/ITR (Information Technology Research) 032518.

References

[1] Wolf S A, Awschalom D D, Buhrman R A, Daughton J M, von Molnar S, Roukes M L, Chtchelkanova A Y and Treger D M 2001 *Science* **294** 1488
[2] Kortright J B, Awschalom D D, Stohr J, Bader S D, Idzerda Y U, Parkin S S P, Schuller I K and Siegmann H-C 1999 *J. Magn. Magn. Mater.* **207** 7
[3] Baibich M N, Broto J M, Fert A, Nguyen Van Dau F, Petroff F, Etienne P, Creuzet G, Friederich A and Chazelas J 1986 *Phys. Rev. Lett.* **61** 2472
[4] Dieny B, Speriosu V S, Parkin S S P, Gurney B A, Wilhoit D R and Mauri D 1997 *Phys. Rev.* B **43** 1297
[5] Grynkewich G, Åkerman J, Brown P, Butcher B, Dave R W, DeHerrera M, Durlam M, Engel B N, Janesky J, Pietambaram S, Rizzo N D, Slaughter J M, Smith K, Sun J J and Tehrani S 2004 *MRS Bull.* **29** 11
[6] Moodera J S and Mathon G 1999 *J. Magn. Magn. Mater.* **200** 248
[7] Mazin I I 1999 *Phys. Rev. Lett.* **83** 1427
[8] Park J-H, Vescovo E, Kim H-J, Kwon C, Ramesh R and Venkatesan T 1998 *Nature* **392** 794
Park J-H, Vescovo E, Kim H-J, Kwon C, Ramesh R and Venkatesan T 1998 *Phys. Rev. Lett.* **81** 1953
[9] Kamper K P, Schmitt W, Guntherodt G, Gambino R J and Ruf R 1987 *Phys. Rev. Lett.* **59** 2788
[10] Morton S A, Waddill G D, Kim S, Schuller I K, Chambers S A and Tobin J G 2002 *Surf. Sci.* **513** L451
[11] Meservey R and Tedrow P M 1994 *Phys. Rep.* **238** 173
[12] de Jong M J M and Beenaker C W J 1995 *Phys. Rev. Lett.* **74** 1657
[13] Upadhyay S K, Palanisami A, Louie R N and Buhrman R A 1998 *Phys. Rev. Lett.* **81** 3247
[14] Soulen R J, Byers J M, Osofsky M S, Nadgorny B, Ambrose T, Cheng S F, Broussard P R, Tanaka C T, Nowak J, Moodera J S, Barry A and Coey J M D 1998 *Science* **282** 85
Soulen R J, Osofsky M S, Nadgorny B, Ambrose T, Broussard P, Cheng S F, Byers J, Tanaka C T, Nowak J, Moodera J S, Laprada G, Barry A and Coey J M D 1999 *J. Appl. Phys.* **85** 4589
[15] Ji Y, Strijkers G J, Yang F Y, Chien C L, Byers J M, Anguelouch A, Xiao G and Gupta A 2001 *Phys. Rev. Lett.* **86** 5585
[16] Anguelouch A, Gupta A, Xiao G, Abraham D W, Ji Y, Ingvarsson S and Chien C L 2001 *Phys. Rev.* B **64** R190408
[17] Nadgorny B, Mazin I I, Osofsky M, Soulen R J, Broussard P, Stroud R M, Singh D J, Harris V G, Arsenov A and Mukovskii Y 2001 *Phys. Rev.* B **63** 184433
[18] Ji Y, Chien C L, Tomioka Y and Tokura Y 2002 *Phys. Rev.* B **66** 012410
[19] Clowes S K, Miyoshi Y, Bugoslavsky Y, Branford W R, Grigorescu C, Manea S A, Monnereau O and Cohen L F 2004 *Phys. Rev.* B **69** 214425
[20] Singh L J, Barber Z H, Miyoshi Y, Bugoslavsky Y, Branford W R and Cohen L F 2004 *Appl. Phys. Lett.* **84** 2367
[21] For broad reviews see, Fang C M, de Wijs G A and de Groot R A 2002 *J. Appl. Phys.* **91** 8340
and Pickett W E and Moodera J S 2001 *Phys. Today* **54** 39
[22] Bratkovsky A M 1998 *Appl. Phys. Lett.* **72** 2334
[23] Bowen M, Bibes M, Barthelemy A, Contour J-P, Anane A, Lemaitre Y and Fert A 2003 *Appl. Phys. Lett.* **82** 233
[24] Hu G and Suzuki Y 2002 *Phys. Rev. Lett.* **89** 276601
[25] Gupta A and Sun J Z 1999 *J. Magn. Magn. Mater.* **200** 24
[26] Fiederling R, Kelm M, Reuscher G, Ossau W, Schmidt G, Waag A and Molenkamp L W 1999 *Nature* **402** 787
[27] Ohno Y, Young D K, Beschoten B, Matsukura F, Ohno H and Awschalom D D 1999 *Nature* **402** 791
[28] Schmidt G, Ferrand D, Molenkamp L W, Filip A T and van Wees B J 2000 *Phys. Rev.* B **62** R4790
[29] Parker J S, Watts S M, Ivanov P G and Xiong P 2002 *Phys. Rev. Lett.* **88** 196601

[30] Dedkov Y S, Rudiger U and Guntherodt G 2002 *Phys. Rev.* B **65** 064417
[31] Braden J G, Parker J S, Xiong P, Chun S H and Samarth N 2003 *Phys. Rev. Lett.* **91** 056602
[32] Dowben P A and Jenkins S J 2005 *Frontiers in Magnetic Materials* ed A V Narlikar (Berlin: Springer) p 295
[33] Skomski R and Dowben P A 2002 *Europhys. Lett.* **58** 544
[34] Itoh H, Ohsawa T and Inoue J 2000 *Phys. Rev. Lett.* **84** 2501
[35] Wang L, Umemoto K, Wentzcovitch R M, Chen T Y, Chien C L, Checkelsky J, Eckert J, Dahlberg E D and Leighton C 2005 *Phys. Rev. Lett.* **94** 056602
[36] Wang L, Chen T Y and Leighton C 2004 *Phys. Rev.* B **69** 094412
[37] Zhao G L, Callaway J and Hayashibara M 1993 *Phys. Rev.* B **48** 15781
[38] Mazin I I 2000 *Appl. Phys. Lett.* **77** 3000
[39] Kwon S K, Youn S J and Min B I 2000 *Phys. Rev.* B **62** 357
[40] Shishidou T, Freeman A J and Asahi R 2001 *Phys. Rev.* B **64** R180401
[41] Ramesha K, Seshadri R, Ederer C, He T and Subramanian M A 2004 *Phys. Rev.* B **70** 214409
[42] Orgassa D, Fujiwara H, Schulthess T C and Butler W H 1999 *Phys. Rev.* B **60** 13237
[43] Tanaka C T, Nowak J and Moodera J S 1999 *J. Appl. Phys.* **86** 6239
[44] Ravel B, Cross J O, Raphael M P, Harris V G, Ramesh R and Saraf V 2002 *Appl. Phys. Lett.* **81** 2812
[45] Kirczenow G 2001 *Phys. Rev.* B **63** 054422
[46] Umemoto K, Wentzcovitch R M, Wang L and Leighton C 2006 *Phys. Status Solidi* b **243** 2117
[47] Bouchard R J 1968 *Mater. Res. Bull.* **3** 563
[48] Ogawa S, Waki S and Teranishi T 1974 *Int. J. Magn.* **5** 349
[49] Cheng S F, Woods G T, Bussmann K, Mazin I I, Soulen R J, Carpenter E E, Das B N and Lubitz P 2003 *J. Appl. Phys.* **93** 6847
[50] Bouchard R J 1968 *J. Cryst. Growth* **2** 40
[51] Takahashi T, Naitoh Y, Sato T, Kamiyama T, Yamada K, Hiraka H, Endoh Y, Usada M and Hamada N 2001 *Phys. Rev.* B **63** 094415
[52] Ogawa S and Teranishi T 1971 *Phys. Lett.* A **36** 407
[53] Ogawa S, Waki S and Teranishi T 1974 *Int. J. Magn.* **5** 349
[54] Yamamoto R, Machida A, Moritomo Y and Nakamura A 1999 *Phys. Rev.* B **59** R7793
[55] Adachi K, Sato K, Okimori M, Yamauchi G, Yasuoka H and Nakamura Y 1975 *J. Phys. Soc. Japan* **38** 81
[56] Wang L, Chen T Y, Chien C L and Leighton C 2006 *Appl. Phys. Lett.* **88** 232509
[57] Willeke G, Dasbach R, Sailer B and Bucher E 1992 *Thin Solid Films* **213** 271
[58] Lichtenberger D, Ellmer K, Schieck R, Fiechter S and Tributsch H 1994 *Thin Solid Films* **246** 6
[59] Hopfner C, Ellmer K, Enanoui A, Pottenkofer C, Fiechter S and Tributsch H 1995 *J. Cryst. Growth* **151** 325
[60] Bronold M, Kubala S, Pettenkofer C and Jaegermann W 1997 *Thin Solid Films* **304** 178
[61] Bausch S, Sailer B, Keppner H, Willeke G, Bucher E and Frommeyer G 1990 *Appl. Phys. Lett.* **57** 25
[62] Meng L, Liu Y H and Tian L 2003 *J. Cryst. Growth* **253** 530
[63] Liu Y H, Meng L and Zhang L 2005 *Thin Solid Films* **479** 83
[64] Wang L, Chen T Y, Chien C L, Checkelsky J G, Eckert J, Dahlberg E D, Umemoto K, Wentzcovitch R M and Leighton C 2006 *Phys. Rev.* B **73** 144402
[65] Hiraka H and Endoh Y 1994 *J. Phys. Soc. Japan* **63** 4573
[66] Byczuk K, Ulmke M and Volhardt D 2003 *Phys. Rev. Lett.* **90** 196403
[67] Jarrett H S, Cloud W H, Bouchard R J, Butler S R, Frederick C G and Gillson J L 1968 *Phys. Rev. Lett.* **21** 617
[68] Iizumi M, Lynn J W, Ohsawa A and Ito H 1975 *AIP Conf. Proc.* **29** 266
[69] McGuire T R and Potter R I 1975 *IEEE Trans. Magn.* **11** 1018
[70] Strijkers G J, Ji Y, Yang F Y, Chien C L and Byers J M 2001 *Phys. Rev.* B **63** 104510
[71] Kuhns P L, Hoch M J R, Reyes A P, Moulton W G, Wang L and Leighton C 2006 *Phys. Rev. Lett.* **96** 167208
[72] Watts S M, Wirth S, von Molnar S, Barry A and Coey J M D 2000 *Phys. Rev.* B **61** 9621